International Journal of Fluid Power 2 (2001) No. 2 pp. 47-63

STATIC-PERFORMANCE BASED COMPUTER-AIDED DESIGN OF A DDV AND ITS SENSITIVITY ANALYSIS

Saikat Mookherjee, Sanjib Acharyya, Kamalesh Majumdar and Dipankar Sanyal

Mechanical Engineering Department, Jadavpur University, Calcutta-700032, India
babun13@hotmail.com

Abstract

Direct Drive valves (DDV) are gaining increasing acceptability for their simple configuration, low leakage, and low cost. Two major components of the present single-stage DDV are a spool valve and a linear force-motor. The objective of the present investigation was to formulate a design methodology and a static performance simulation tool for the DDV. The present work includes lumped and chiefly one-dimensional, non-linear field modelling of flow through the spool valve and magnetic flux in the motor. Detail modelling has been done only for leakage flow in the spool-bushing radial clearance of the spool valve, since it has critical bearing in the performance analysis. A computer-aided tool for designing a single stage valve, based on some additional simplifying assumptions of the lumped model, has been presented. The static performance algorithm was developed on SIMULINK, without invoking the design-level simplifications. The simulation tool has been used to carry out a design validation against the known performance of Moog Series D633 valve. Different designs of the valve, corresponding to different actuation specifications were obtained, and their static performances have been investigated. Also a sensitivity analysis has been carried out to study the effects of tractive air gap area ratio in the motor and port lap conditions in the spool valve.

Keywords: direct drive valve, linear force motor, spool valve, flow gain, pressure gain, design, static performance analysis, sensitivity analysis

1 Introduction

An Electro-Hydraulic Servovalve (EHSV) is an essential item of servomechanism where fast speed of response, high power output and working fidelity are necessary. A single-stage electrohydraulic Servovalve is commonly known as Direct Drive Valve (DDV). The DDV consisting of a linear force-motor (LFM) driving a spool valve directly, controls flow from a pump to an actuator. The component profile of a DDV is much simpler in comparison to a two-stage EHSV with a hydraulic amplifier and feedback wire (Moog, 1965). Miller (1993) observed that with development in both solid-state devices and new magnetic materials with higher power density, research in DDV technology is becoming increasingly important. This is due to its low leakage, simplicity in manufacturing and low cost in comparison to a two-stage valve. Steed (1993) suggested increased investigations into the capabilities of DDV to make the technology even more widely applicable. In a recent publication, Jones (1997) opined that a great deal of research with servo-electronics in loop is aimed at to make a DDV perform as good as a two-stage valve.

Design and performance study of such a valve involves detailed modelling of both the electromagnetic fluxes in the motor and flow through the spool valve. Lee and Blackburn (1952) proposed a mathematical model to predict the steady-state flow force for flow past a square edge due to non-radial jets in the spool valve. Merritt (1967) provided an account of analyzing the magnetic circuit of a particular torque-motor configuration. Saha et al (1998) presented the conceptual design of a force motor driven single-stage DDV. Mookherjee (2000) presented the detailed mathematical modelling of the main flows in the spool valve and the electromagnetic flux in the Linear Force Motor, hereon also designated as LFM, A preliminary design procedure and sensitivity analysis results for a DDV was also presented. An underlapped valve was found to deliver higher control flow than an overlapped valve, due to lesser resistance in the main flow path. Increased non-linearity with radial clearance was attributed to persistence of jet-angle variation over larger spool displacement. Port shaping was proposed to be effective to counteract the motor non-linearity.

This manuscript was received on 15 November 2000 and was accepted after revision for publication on 26 June 2001

The principle objective of this investigation was to develop on to the design tool, presented by Mookherjee (2000), for a DDV and make a critical evaluation of its acceptability. The mathematical models of Mookherjee (2000), along with some simplifications, are used to develop a computer-aided design methodology. Following the design procedure, the geometrical sizes and other details of the different items of the valve are obtained.

A computer-aided static performance simulation tool is evolved on SIMULINK, based on the detailed modelling dispensing with the design level simplifications. A modelling of the leakage flow in the spool-bushing radial clearance of the spool valve was developed for the purpose. The static performance results for different designs of the DDV corresponding to different actuation specifications are investigated. The tool is also used to carry out a sensitivity analysis followed by a design validation against the known performance of a Moog Series D633 valve. An objective of the sensitivity analysis is to study the effects of geometrical sizes on the static performance of the valve. This study is essential for identification of tolerance limits of component sizes within the satisfactory range of valve performance.

2 Function

A schematic of the DDV - comprising of an LFM and a spool valve - is given in Fig. 1. At null condition, defined as zero coil current and the four tractive air-gaps equal to g_o, the ring type armature of the LFM posseses static equilibrium. An impressed voltage causes a current in the coil to build up and attain a new steady state depending on air-gap impedance and coil resistance. This results in a magnetic field which, on interacting with the field due to the permanent magnets, generates a force, F_{em} causing the armature-spool assembly to move. The mechanical springs resist displacement by exerting a restoring force, F_{mech}. The residual force is responsible for motion of the spool, and under static condition of say, displacement x, equals the steady-state flow force F_S due to flow from supply pressure P_S and return pressure P_R. These forces are shown in Fig. 2.

For the displacement x, of the spool away from the LFM end, with reference to Fig. 1 and 2, ports p_1 and p_4 are uncovered, while ports p_2 and p_3 get closed. This results in main flows Q_1 and Q_4, and leakage flows, Q_2 and Q_3. Flows to and from the actuator - Q_{c1} and Q_{c2} - are termed as control flows. The pressure difference
(P_1 - P_2), across a symmetric actuator piston is termed as load pressure, designated by P_L. A symmetric no-load actuator implies a zero value for the load pressure and the corresponding control flow is said to be the no-load control flow. The stationary condition of the actuator is called locked actuator and then, $Q_{c1} = Q_{c2} = 0$. The control flow and the leakage flow together constitute the valve flow Q_v.

3 Design-Level Mathematical Model of Spool Valve

Unless otherwise mentioned in the present analysis, all the port cuts have been assumed to be rectangular, identified by a constant width, w/n_P and constant wrap angle, θ_P/n_P, subtended at the axis of the spool valve by each cut, as shown in Fig. 2(b). This figure illustrates a special case of $n_P = 4$ for each port. The supply and return pressures have been assumed constant. The locations where significant pressure drops occur along the flow path have been assumed to be only at the small port openings of the spool valve. The other assumptions made in the present mathematical modelling are symmetric ports, incompressible fluid and negligible pressure loss in the hydraulic lines. These assumptions are also inherent in the modelling for the detailed static performance analysis.

The design model of the DDV makes use of further assumptions that are relaxed in the model for static performance analysis. These additional design-level assumptions are identical pair of permanent magnets, geometrically similar air-gaps and pole-pieces, critically lapped spool valve and identical port geometries of metered ports. The effect of leakage flow is considered negligible in the rated valve flow. These assumptions are discussed at appropriate places of this section, to follow.

3.1 Pressure – Velocity – Discharge Relations

With reference to Fig. 2(a), for spool displacement x from null and a general case of port underlap 'u', the effective port openings at the four metered ports p_i (i = 1 to 4), are expressed as,

$$X_i = u + x, \text{ for i = 1 and 4} \tag{1a}$$

$$X_i = u - x, \text{ for i = 2 and 3} \tag{1b}$$

The turbulent flow through the uncovered ports is usually modeled with a constant discharge coefficient C_{dp} and velocity coefficient C_{vp}, both of which depend on the neighborhood geometry. It is imperative that only at the design level, the underlap value has been assumed as zero. The pressure-velocity and pressure-discharge relations corresponding spool displacement x, for the i^{th} port are

$$V_i = C_{vp}\sqrt{\frac{2(-1)^{k+1}\left(P^{(k)} - P_m\right)}{\rho}} \tag{2}$$

$$Q_i = C_{dp} w\left[X_i \sin\alpha_i + r_c \cos\alpha_i\right] \cdot\sqrt{\frac{2(-1)^{k+1}\left(P^{(k)} - P_m\right)}{\rho}} \tag{3}$$

where ρ is the density of the fluid and α_i is the angle of discharge for the i^{th} port. In the above equations, k = 1 if i = 1 or 3 and k = 2 if i = 2 or 4 . Also, $P^{(1)} = P_S$ and $P^{(2)} = P_R$ P_m indicates the chamber pressures, with m = 1 or 2.

The projected length $[X_1\sin\alpha_1 + r_c\cos\alpha_1]$ of open port 1, in the direction perpendicular to jet flow at

port 1, and the port width *w*, are clearly depicted in Fig. 2(a) and 2(b) respectively.

The corresponding jet angle α_i at any port p_i depends on the ratio X_i/r_c (Merritt, 1967), where r_c is the spool-bushing radial clearance. This clearance is small by more than one order compared to the rated stroke of the valve. The two extreme values of the jet angle are

$$\alpha_i = 69° \text{ for } X_i/r_c >> 1 \text{ and} \quad (4a)$$

$$\alpha_i = 21^0 \text{ for } X_i/r_c = 0 \quad (4b)$$

For rectangular port cuts, it is customary to take $C_{vp} = 0.98$ and $C_{dp} = 0.6$ (Yeaple, 1996).

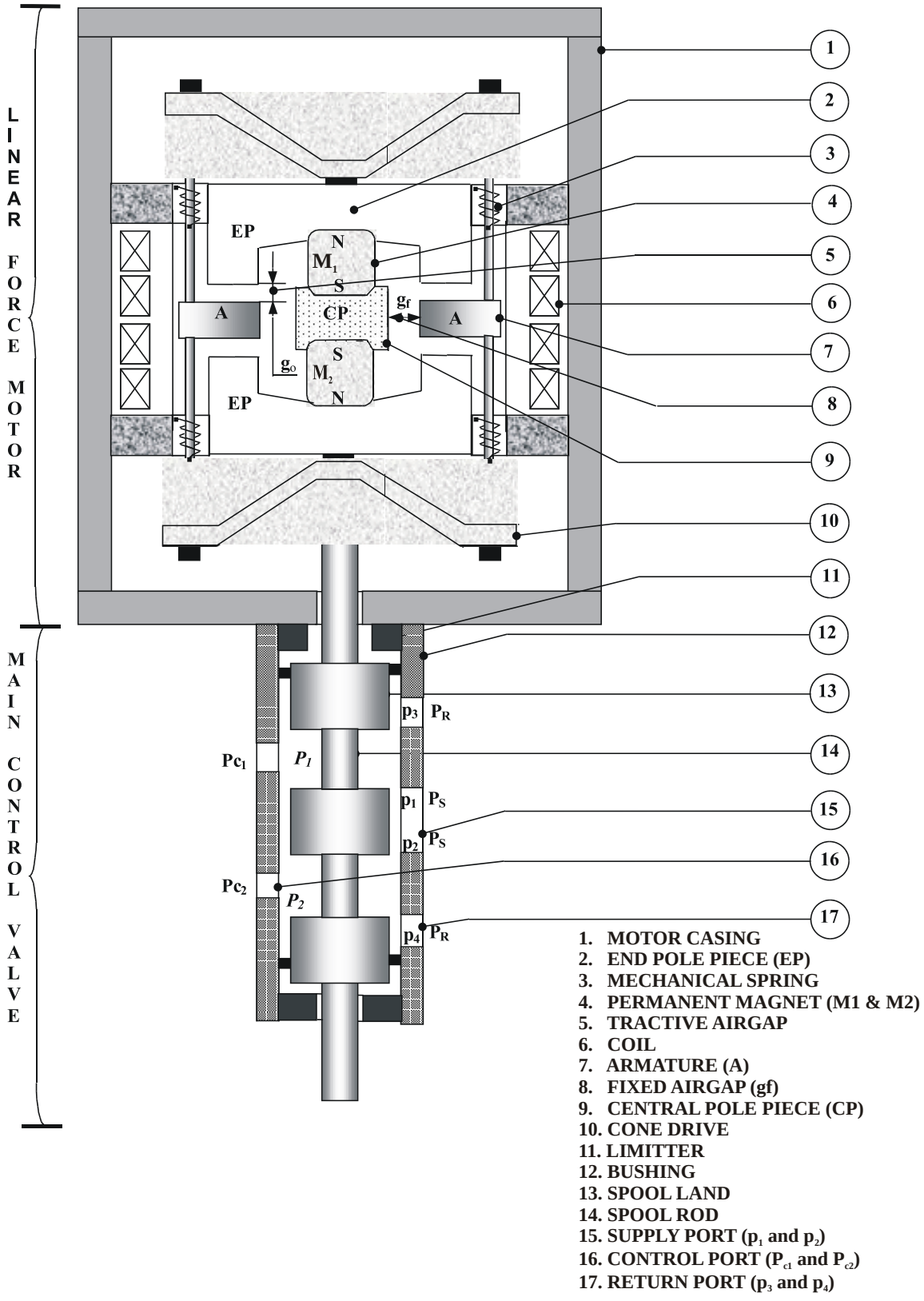

Fig. 1: *Schematic of a Direct Drive Valve*

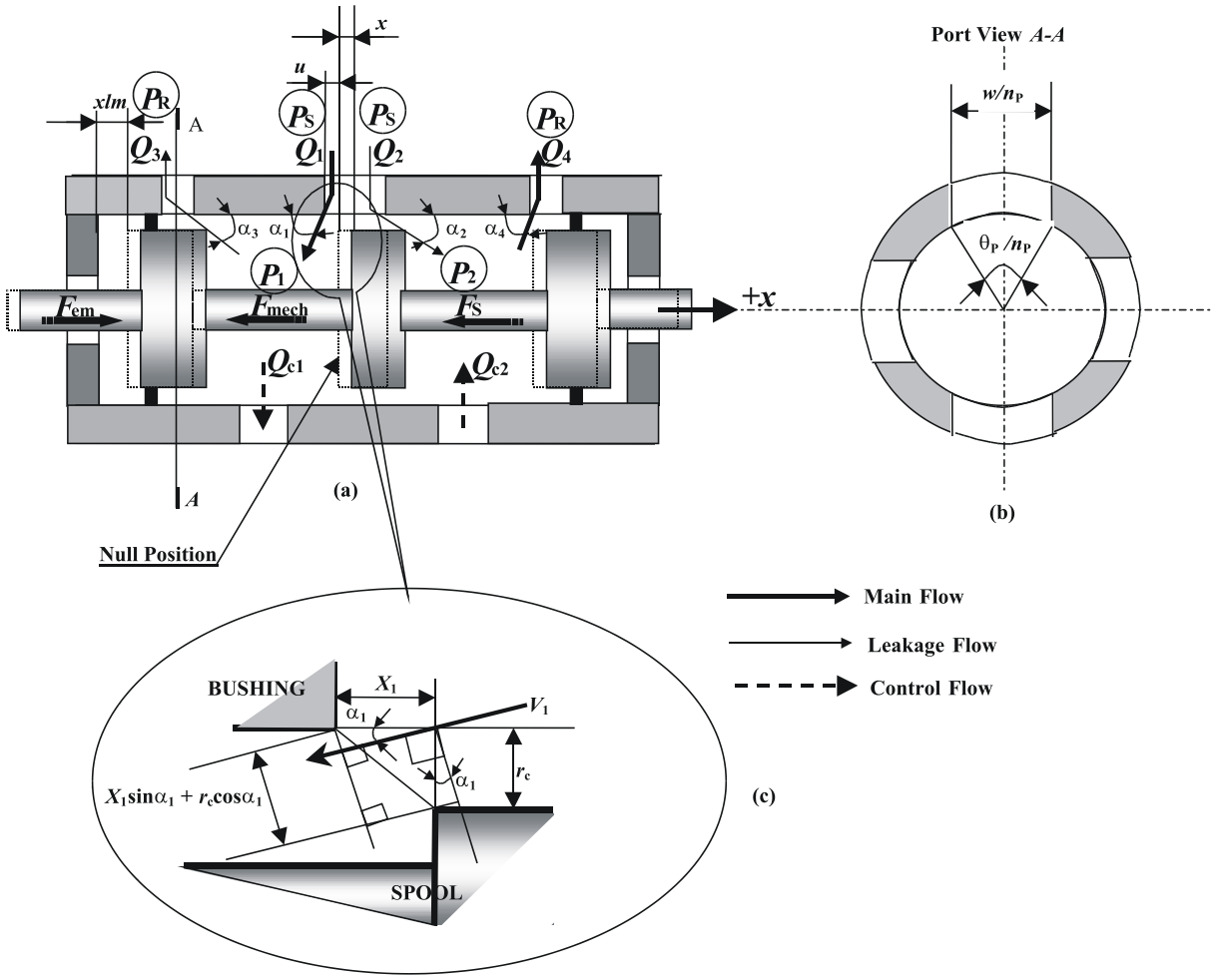

Fig. 2: *Flow Detail through a Spool Valve*

The relationship between port width w and the port wrap angle θ_P, can be obtained from the port geometry as

$$w = 0.5 d_s \theta_P \text{ , for } X_i < 0.0 \tag{5}$$

where d_s represents the spool diameter, and n_P is the number of port cuts per port.

In the design procedure, neglecting flow leakage through spool valve, the rated valve flow and the control flow at $x = x_s$ can be expressed as,

$$Q_v = Q_{c1} = Q_{c2} = Q_1\,(x = x_s) = Q_4\,(x = x_s) \tag{6}$$

where x_s is the steady-state displacement of the spool at which no-load rated discharge through the valve is obtained. Similarly, the maximum leakage flow at null can be expressed for a critically lapped valve as,

$$Q_L\big|_{max} = Q_1(x = 0) + Q_2(x = 0) \tag{7}$$

Equations 6 and 7 are used in combination with Eq. 3. The jet angles in these cases are respectively taken from Eq. 4b and 4c.

For the design model, corresponding to the no-load case and geometrically similar ports, the chamber pressures can be expressed as,

$$P_1 = P_2 = (P_S + P_R)/2 \tag{8}$$

3.2 Steady State Flow Force on spool

As depicted in Fig. 2(a), because of flow turning, an axial force is exerted on the spool in the direction of turning of jet at each port. In view of the four such jets, the net steady-state flow force acting on the spool in the direction opposite to spool displacement can be expressed as:

$$F_S = F_{S1} - F_{S2} - F_{S3} + F_{S4} \tag{9}$$

The numerical subscripts in the above equation refer to port locations, and a negative sign implies a force in the direction of spool displacement. Applying conservation of linear momentum principal, the above equation can be rewritten as,

$$F_S = \rho\left(Q_1V_1\cos\alpha_1 - Q_2V_2\cos\alpha_2 - Q_3V_3\cos\alpha_3 + Q_4V_4\cos\alpha_4\right) \tag{10}$$

For the design model, at the rated x_s, the contributions of the leakage paths (2 and 3) have been neglected.

In the analysis model for steady state performance, this force can be evaluated after solving the pressure-discharge relations for all the flow paths through the spool valve, as already described in the previous section.

4 Mathematical Model of LFM

The magnetic material chosen for LFM is Samarium-Cobalt (Sm_2Co_2). Its demagnetising curve is linear up to a high temperature and characterised by high residual flux density, B_o = 1.1 Wb/m^2 and large coercivity, $H_o = 7.5 \cdot 10^5$ AT/m.

Following the analysis by Mookherjee (2000), the expression of the electromagnetic force of the armature can be expressed as

$$F_{em} = \frac{H_o L_m / B_o A_m}{\left(\frac{2 g_o g_f}{\mu^2 A_t A_f} + \frac{g_o^2}{\mu^2 A_t^2} - \frac{x^2}{\mu^2 A_t^2} + \frac{g_o^2}{\mu^2 A_t^2} + \frac{g_o H_o L_m}{\mu A_t B_o A_m} \right)} \cdot \left[\left(\frac{4 H_o^2 g_o L_m^2}{\mu^2 A_t^2} \right) x + \left(\frac{2 H_o L_m N}{\mu^2 A_t^2} \right) x^2 + \left\{ \frac{2 H_o g_o L_m N}{\mu A_t} \left(\frac{H_o L_m}{B_o A_m} + 2 \frac{g_f}{\mu A_f} + \frac{g_o}{\mu A_t} \right) \right\} c + \left\{ \frac{N^2}{\mu A_t} \left(\frac{H_o L_m}{B_o A_m} + 2 \frac{g_f}{\mu A_f} + \frac{g_o}{\mu A_t} \right) \right\} c^2 x \right] \quad (11)$$

The above expression is obtained for a matched pair of magnets of length L_m and cross-sectional area A_m and a matched pair of tractive air gaps of identical area A_t. In the above equation g_o and g_f are the tractive air gap and fixed air gap lengths respectively, A_f is the fixed air gap area, x and c are the armature displacement and coil current respectively and N is the number of coil turns. Equation (11) indicates non-linear variation of the force with respect to both spool displacement and coil current.

5 Design Methodology

The aim of the design methodology on the basis of no-load and locked steady-state requirements of the DDV is to provide a simple way of obtaining the design output. To be consistent with the aim, equations are further simplified through some design-level assumptions. Four user-specified requirements of the present design are: constraint on permissible envelope size of the LFM, the maximum permissible coil resistance, inner diameter of the hollow magnets and the total port wrap angle. The requirements emerging from physics are

- chip shear force requirement for chip removal at any cut of the spool valve port,
- rated no-load valve flow,
- maximum permitted no-load hydraulic leakage,
- coil design within permissible envelope size for LFM,
- magnet design for chip shear force capability of LFM and operation of magnets without undergoing unwarranted demagnetization at extreme conditions of armature movement and coil current,
- operation of magnets at maximum flux density point at null,
- LFM force capability at steady-state of no-load rated valve flow and rated coil current condition, and
- unique steady position for all currents by the use of mechanical limiter

5.1 Design of metered ports

The design of the spool valve begins with the estimation of the sizes of the metered ports, as illustrated in Fig. 4. Each of the four metered ports are considered to be made of a number of rectangular cuts together subtending a total wrap angle θ_P of 128^o at the spool axis. Number of cuts for each metered port is obtained from the evaluated chip shear force F_{CS} and specified valve flow and pressure across the valve as

$$n_P = 0.81 \frac{\left(\frac{Q_V}{C_{dp} \sqrt{(P_S - P_R)/\rho}} \right)}{\left(F_{cs} / \tau_{cs} \right)} \quad (12)$$

rounded up to the next even integer.

The requirement of chip shear force arises out of shearing the chips off, if produced or entered within the DDV, at any single cut in a metered ports. Miller (1993) suggested calculation based on most possible adverse condition of 81 % of the area of any cut covered by a chip entering radially into the spool valve. This explains the numeric constant in the above equation. The numerator fraction is the circumferential area at steady-state port opening comprising all cuts. The denominator fraction is the maximum area that can be sheared by the force F_{CS}. This force, whose estimation is a prerequisite of using Eq. 12, is generated on passing maximum permissible current c_{max}, through the coils in the LFM. It is customary to write

$$F_{CS} = F_{em} (c = c_{max}, x = 0) \quad (13)$$

The spool driving force contributed by the LFM has three parts. A part of this force is due to the coil current. The other part of the force from the LFM is due to increased magnetic force of attraction in the direction of armature displacement. The corresponding force coefficient is termed as magnetic stiffness. This is a decentering contribution in contrast to the third part of the spool driving force, which is a centering contribution due to mechanical spring. With increase in steady-state armature displacement from its null, the spool driving force for a constant current droops due to domination of the mechanical spring in that range of displacement. For larger displacement, the trend is reversed due to larger magnetic spring force. Therefore, it is possible to have two possible steady-states. These positions correspond to the balance of the spool driving force and the steady-state flow force, which is a monotonically increasing force with armature displacement. Excluding the possibility of motion up to second steady state, by placing a mechancial limiter between the two possible steady state positions, allows settling to only a unique steady-state. This is attained after the expected dynamic overshoots and undershoots of armature movement subside. This is because even during the dynamic overshoot past the first steady-state, the spool

may move only up to a maximum allowed by the mechanical limiter. All these design aspects are highlighted later in Fig. 12, in terms of the designed valve. A good separation of the two steady-states is necessary to minimise the intensity of limiter hitting during dynamic overshoot of the armature-spool assembly. This necessitates the first steady-state to fall in the drooping domain of the driving force curve. Thus, it can be written that

$$F_{em}\,(c = c_r,\, x = 0) > F_S\,(x = x_s) \tag{14}$$

where, c_r is the rated coil current.

For design, it is initially chosen that,

$$\frac{c_r}{c_{max}} F_{em}(c = c_{max},\, x = 0) = 1.2\, F_S(x = x_s) \tag{15}$$

where using Eq. 1 with u = 0, Eq. 2, 3, 4b, 8 and 10, the steady-state flow force at rated stroke can be obtained in design as

$$F_S\left(x = x_s\right) = 2C_{dp}C_{vp}n_P d_s \sin\frac{\theta_P}{2n_P}$$

$$\cdot\, x_s \sin 69^o \cos 69^o \left(P_S - P_R\right) \tag{16}$$

5.2 Design of the spool

The spool interland diameter d_i, is estimated from the machinability condition. An initial assumption made in the design of spool is the ratio of mechanical limiter size to rated spool stroke, $xlm\,/x_s$, to be equal to 3.0. Both the annular flow area within the spool and full circumferential flow areas upstream and downstream of the supply and return port openings respectively, have been assumed to be 3.5 times larger (Merritt, 1967) than the total metered port area at the maximum spool stroke equal to the limiter size. This assumption has been made to ensure that the major pressure drop within the spool valve occurs at the port openings only. Hence, for a critically lapped valve, using Eq. 3, 4b, 6 and 8, it can be written that

$$\frac{\pi}{4}\left(d_s^2 - d_i^2\right) = 3.5\left(\frac{xlm}{x_s}\right)\frac{Q_c}{\sin 69^o C_{dp}\sqrt{\left(P_S - P_R\right)/\rho}} \tag{17}$$

where Q_c is the rated control flow. The spool diameter d_s is obtained from the above equation.

The rated spool stroke is obtained for the rated no-load control flow which can be obtained from Eq. 3, 4b, 5 and 6 as,

$$x_s = \frac{\left(\dfrac{Q_c}{\sin 69^o C_{dp}\sqrt{\left(P_S - P_R\right)/\rho}}\right)}{n_P d_s \sin\left(\dfrac{\theta_P}{2n_P}\right)} \tag{18}$$

The spool - bushing radial clearance r_c is obtained from the expression of the specified maximum permissible leakage flow at null, which can be expressed from Eq. 3, 4c, 7 and 8 as

$$Q_{L_{max}} = 2C_{dp}\sqrt{\frac{(P_S - P_R)}{\rho}}\, n_P d_s \sin\frac{\theta_P}{2n_P} r_c \sin 21^o \tag{19}$$

5.3 Coil Design within Permissible Envelope Size for LFM

The starting point of the LFM design algorithm is to design the coil corresponding to the maximum permissible resistance R_{max} within the permissible envelope size. The length of the coil bobbin L_{cl}, inner and outer coil bobbin diameters - d_{clbi} and d_{clbo}, number of coil turns N, are designed as discussed by Mookherjee (2000).

5.4 Magnet Design for Chip Shear Force Capability and Non-demagnetization

The conditions of minimum and maximum permissible flux conditions without demagnetization of the permanent magnets, yield

$$H_o L_m \geq N\, c_{max} \tag{20}$$

The magnet length is evaluated at this stage considering the above equation as

$$H_o L_m = N\, c_{max} \tag{21}$$

The magnet inner diameter d_{mi} is assumed as 1mm and outer diameter is calculated from the area obtained for the given chip shear force condition at maximum coil current and null armature position, i.e.,

$$F_{cs} = \left.\frac{\partial F_{em}}{\partial c}\right|_{x=0} c_{max} = \frac{B_o A_m N c_{max}}{g_o} \tag{22}$$

and

$$A_m = \pi\left(d_{mo}^2 - d_{mi}^2\right) \tag{23}$$

It may be noted here that the design presented here considers matched pair of magnets. Hence, for brevity the subscripts are omitted, which are otherwise used for identifying the difference in a general case.

5.5 Air-gap design for operation of Magnets at maximum flux density point at null

For operating at the maximum magnetic power density point corresponding to geometric null condition, the magnetic fluxes can be written as

$$\psi_{1o} = \psi_{2o} = \psi_o = 0.5 B_o A_m \tag{24}$$

and

$$M_1 = M_2 = M_o = 0.5 H_o L_m \tag{25}$$

Considering Eq. 25 and the electromagnetic network analysis (Mookherjee, 2000), it is obtained that

$$\psi_o = \frac{M_o}{\left(\dfrac{2g_f}{\mu A_f} + \dfrac{g_o}{\mu A_t}\right)} \tag{26}$$

or,
$$\frac{H_o L_m}{B_o A_m} = \frac{2g_f}{\mu A_f} + \frac{g_o}{\mu A_t} \tag{27}$$

The tractive and fixed air-gap areas can be respectively expressed as

$$A_t = \frac{\pi\left\{\left(d_{clbi} - d_p - 2c_p\right)^2 - \left(d_{clbi} - d_p - 2c_p - t_a\right)^2\right\}}{4} \quad (28)$$

$$A_f = \pi (d_{clbi} - t_a - d_p - 2c_p) L_a \quad (29)$$

where the pole piece sizes are evaluated from the last three equations within the available space between the magnet and the coil bobbin. In the above equations, d_p, c_p, t_a and L_a refer to the diameter of the pushrod, clearance around pushrod, armature thickness and armature length respectively. This requires solving a nonlinear equation at this stage through the Newton-Raphson method. If any geometrical size is negative or unacceptably small following this stage, the algorithm loops back first to magnet design, only to increase magnet length and then to the coil design with a reduced envelope size, if required.

5.6 LFM Force Capability for Steady State Rated Valve Flow Condition

The force equilibrium between the spool, the armature and the mechanical springs corresponding to the no-load rated valve flow at rated coil current is given by following equations.

$$F_{em}\left(c = c_r,\, x = x_s\right) = F_S\left(x = x_s\right) + K_{mech}\, x_s \quad (30)$$

where K_{mech} is the stiffness of the mechanical spring. The stiffness of the mechanical spring is designed from the above equation.

5.7 Design of the mechanical limiter

It should be noted that the limiter position should be such that the following considerations are met in the design.

- The limiter position should be beyond the rated no-load stroke.
- There cannot be more than one steady-state corresponding to the rated current.
- The mechanical spring stiffness should be sufficient for armature retraction from the mechanical limiter without flow through the spool valve and no coil current.

In order to achieve these conditions, the initial assumption regarding the limiter size calls for modification. Redesigning the DDV, starting from the spool is repeated till a convergence of the limiter size is achieved. The overall design algorithm is shown in Fig.4 in a self-explanatory manner.

6 Design Results

Design results are obtained from specification, enlisted in Table 1, following an iterative scheme, as depicted in Fig. 3. Four different cases of pressure and flow conditions have been considered in the design, which are presented below:

Case I : P_S = 22.5 MPa; Q_c = 2.0 $\cdot 10^{-3}$ m^3/s
Case II : P_S = 30.0 MPa; Q_c = 1.5 $\cdot 10^{-3}$ m^3/s
Case III : P_S = 45.0 MPa; Q_c = 1.0 $\cdot 10^{-3}$ m^3/s
Case IV : P_S = 7.0 MPa; Q_c = 0.66 $\cdot 10^{-3}$ m^3/s

The first three cases correspond to results discussed in Section 10. The last case corresponds to the specification of the Moog series D633 DDV, which provides a case for validation of the present design algorithm vis-a-vis a sensitivity analysis, presented in Section 11. The design specifications are given in Table 1. Some of the changes corresponding to the Moog series D633 DDV are indicated in Table 1 after the slash. Table 2 provides the design sizes obtained from the present algorithm.

Table 1: Design Specifications

Specifications	Unit	Value
Pump supply pressure	[MPa]	stated above
Return pressure	[MPa]	0
Magnetic permeability air	[H/m]	$1.256 \cdot 10^{-6}$
Retentivity of magnets	[Wb/m^2]	1.1
Field strength of magnet	[AT/m]	$7.5 \cdot 10^{5}$
Resistance/length of magnet material	[Ω/m]	0.0086
Envelope outer diameter	[m]	0.08/0.14
Envelope length	[m]	0.075/0.1
Fluid density	[kg/m^3]	840
Fluid viscosity	[Pa·s]	$4.3 \cdot 10^{-3}$
Shear strength of chip	[N/m^2]	$6.2 \cdot 10^{8}$
Rated valve flow	[m^3/s]	stated above
Maximum no-load leakage	[m^3/s]	$5 \cdot 10^{-5}$/1.410^{-5}
Resistivity of coil wire	[Ω/m]	0.104
Diameter of bare wire	[m]	$4 \cdot 10^{-4}$
Thickness of insulation	[m]	$3.1 \cdot 10^{-5}$
Maximum permissible resistance	[Ω]	8/6
Number of coil bobbins	[-]	4
Rated current	[A]	1.0/1.2
Maximum current	[A]	3.0/3.6

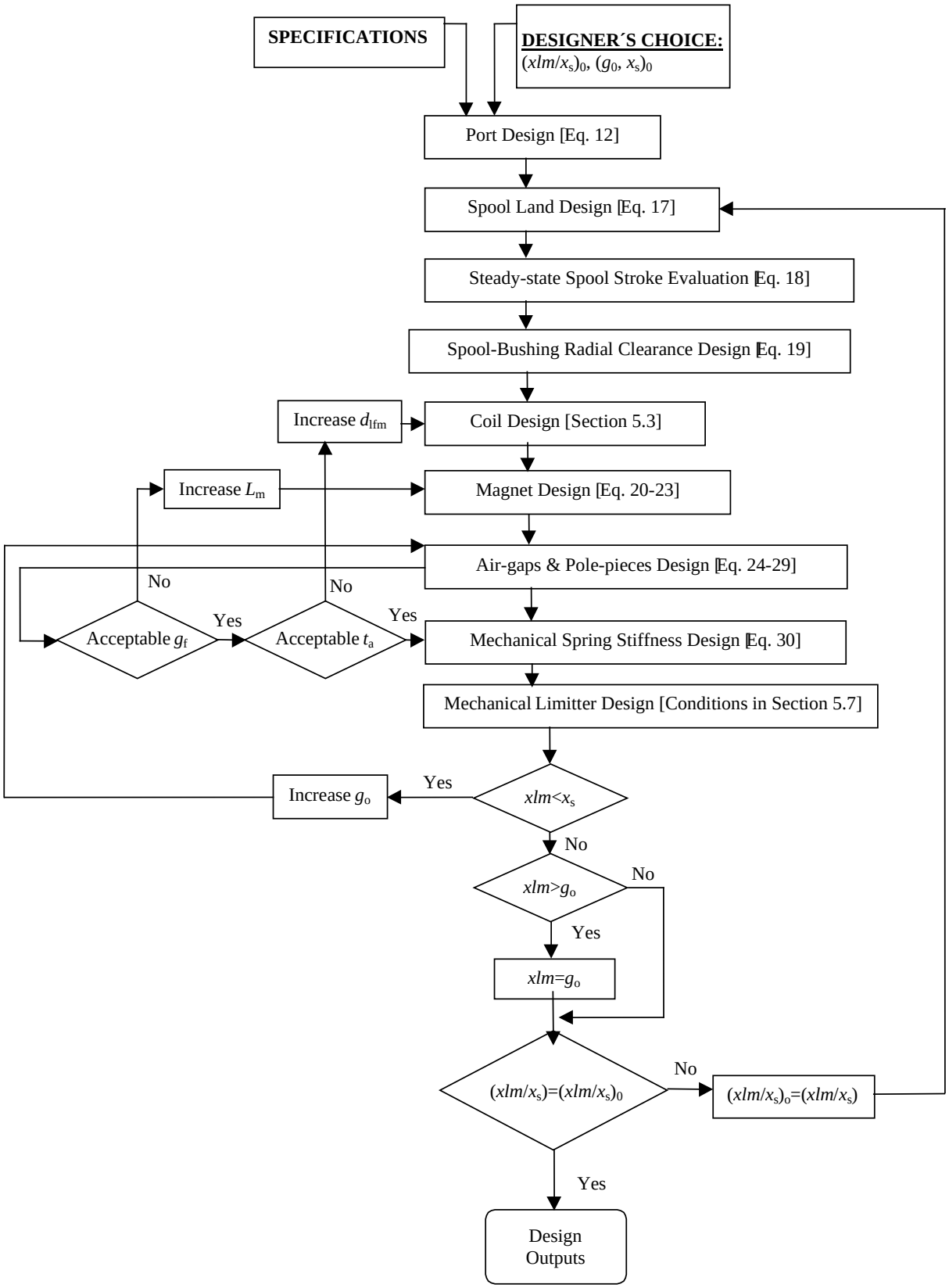

Fig. 3: *The Design Algorithm*

Table 2: Design Results

Designed Variables	Units	Case I	Case II	Case III	Case IV
Magnet outer diameter	[m]	$3.31 \cdot 10^{-2}$	$2.68 \cdot 10^{-2}$	$1.96 \cdot 10^{-2}$	$6.67 \cdot 10^{-2}$
Magnet inner diameter	[m]	$1 \cdot 10^{-3}$	$1 \cdot 10^{-3}$	$1 \cdot 10^{-3}$	$1 \cdot 10^{-3}$
Magnet length	[m]	$1.64 \cdot 10^{-2}$	$1.64 \cdot 10^{-2}$	$1.64 \cdot 10^{-2}$	$7.85 \cdot 10^{-3}$
Armature length	[m]	$1.82 \cdot 10^{-2}$	$1.14 \cdot 10^{-2}$	$3.7 \cdot 10^{-3}$	$2.9 \cdot 10^{-2}$
Armature outer diameter	[m]	$6.1 \cdot 10^{-2}$	$6.1 \cdot 10^{-2}$	$6.1 \cdot 10^{-2}$	$1.27 \cdot 10^{-1}$
Armature inner diameter	[m]	$3.96 \cdot 10^{-2}$	$3.46 \cdot 10^{-2}$	$2.44 \cdot 10^{-2}$	$6.98 \cdot 10^{-2}$
Tractive Air-gap length at null	[m]	$2.8 \cdot 10^{-3}$	$2.12 \cdot 10^{-3}$	$1.38 \cdot 10^{-3}$	$3.8 \cdot 10^{-3}$
Tractive Air-gap thickness	[m]	$6.1 \cdot 10^{-3}$	$7.4 \cdot 10^{-3}$	$1.55 \cdot 10^{-2}$	$2.77 \cdot 10^{-2}$
Fixed Air-gap Thickness	[m]	$2.3 \cdot 10^{-3}$	$2.9 \cdot 10^{-3}$	$1.4 \cdot 10^{-3}$	$5.4 \cdot 10^{-4}$
Central Polepiece length	[m]	$1.62 \cdot 10^{-2}$	$9.97 \cdot 10^{-3}$	$2.77 \cdot 10^{-3}$	$2.56 \cdot 10^{-2}$
Central Polepiece outer diameter	[m]	$3.51 \cdot 10^{-2}$	$2.9 \cdot 10^{-2}$	$2.16 \cdot 10^{-2}$	$6.87 \cdot 10^{-2}$
End Polepiece length at centerline	[m]	$6.1 \cdot 10^{-3}$	$7.4 \cdot 10^{-3}$	$1.55 \cdot 10^{-2}$	$2.78 \cdot 10^{-2}$
End Polepiece length at outer rim	[m]	$2.13 \cdot 10^{-2}$	$2.34 \cdot 10^{-2}$	$1.92 \cdot 10^{-2}$	$6.73 \cdot 10^{-3}$
End Polepiece outer diameter at airgap	[m]	$5.64 \cdot 10^{-2}$	$5.52 \cdot 10^{-2}$	$5.81 \cdot 10^{-2}$	$1.26 \cdot 10^{-1}$
Coil length of wire per coil	[m]	77.0	77.0	77.0	58.0
Coil bobbin length per coil	[m]	$1.617 \cdot 10^{-2}$	$1.617 \cdot 10^{-2}$	$1.617 \cdot 10^{-2}$	$2.26 \cdot 10^{-2}$
Coil bobbin inner diameter	[m]	$6.7 \cdot 10^{-2}$	$6.7 \cdot 10^{-2}$	$6.7 \cdot 10^{-2}$	$1.33 \cdot 10^{-1}$
Coil bobbin outer diameter	[m]	$7.6 \cdot 10^{-2}$	$7.6 \cdot 10^{-2}$	$7.6 \cdot 10^{-2}$	$1.36 \cdot 10^{-1}$
Spool land diameter	[m]	$1.9 \cdot 10^{-2}$	$1.8 \cdot 10^{-2}$	$1.5 \cdot 10^{-2}$	$1.1 \cdot 10^{-2}$
Spool inter-land diameter	[m]	$1.05 \cdot 10^{-2}$	$1.05 \cdot 10^{-2}$	$1.05 \cdot 10^{-2}$	$5.0 \cdot 10^{-3}$
Spool total length	[m]	$1.98 \cdot 10^{-1}$	$1.65 \cdot 10^{-1}$	$1.1 \cdot 10^{-1}$	$1.76 \cdot 10^{-1}$
Spool supply land length	[m]	$1.8 \cdot 10^{-2}$	$1.5 \cdot 10^{-2}$	$1 \cdot 10^{-2}$	$1.6 \cdot 10^{-2}$
Spool non-supply land length	[m]	$3.6 \cdot 10^{-2}$	$3 \cdot 10^{-2}$	$2 \cdot 10^{-2}$	$3.2 \cdot 10^{-2}$
Spool chamber length	[m]	$1.8 \cdot 10^{-2}$	$1.5 \cdot 10^{-2}$	$1 \cdot 10^{-2}$	$1.6 \cdot 10^{-2}$
Spool steady-state stroke	[m]	$1.03 \cdot 10^{-3}$	$7.06 \cdot 10^{-4}$	$4.62 \cdot 10^{-4}$	$1.742 \cdot 10^{-3}$
Spool-Bushing radial clearance	[m]	$1.3 \cdot 10^{-5}$	$1.2 \cdot 10^{-5}$	$1.15 \cdot 10^{-5}$	$1.84 \cdot 10^{-5}$
Number of port cuts	[-]	16	12	8	8
Limiter length	[m]	$2.57 \cdot 10^{-3}$	$2.12 \cdot 10^{-3}$	$1.38 \cdot 10^{-3}$	$2.2 \cdot 10^{-3}$
Mechanical Spring stiffness	[N/m]	$2.2 \cdot 10^{5}$	$1.42 \cdot 10^{5}$	$9.68 \cdot 10^{4}$	$4.37 \cdot 10^{5}$

7 Mathematical Model for Spool Valve Flow for Static Performance Analysis

Static performance configuration implies a constant current in the coils leading to a steady position of the spool resulting in a constant slewing rate of the actuator piston. In Section 4, modelling the main flows, Q_1 and Q_4, and their contribution to flow force have already been addressed. Here, the modelling of the leakage flows Q_2 and Q_3, along with their contribution to the steady state flow force, are presented. If the flow in the leakage path through the spool-bushing radial-clearance, r_c becomes fully developed, then in the present analysis, it has been referred to as flow through a long orifice. The exploded view of flow for a general case presented in Fig. 5 depicts such a case. For brevity, the subscripts for different ports are omitted in the present discussion. This generalisation also keeps the analysis ready for application for the computation of pressure drop in transmission lines of short length. The length of the flow path in the spool-bushing radial clearance beyond which the flow is fully developed has been described here as large transition length, x_{tl}. The fully developed flow analysis through an annular duct is well known (Bird et al, 1960). If the effective port opening X is greater than x_{tl}, then based on fully developed steady laminar flow analysis through an annular orifice of small radial width, the average velocity and discharge can be expressed as,

$$V = \left(r_c^2 \, \Delta P\right) / \left(12 \mu_f \, X\right) \tag{31}$$

$$Q = \left(d_s \, \theta_P \, r_c^3 \, \Delta P\right) / \left(24 \mu_f \, X\right) \tag{32}$$

Here d_s is the spool land diameter, ΔP is the pressure drop across the leakage path, θ_P is the port wrap angle, shown in Fig. 2(b), μ_f is the fluid viscosity and r_c is the spool-bushing radial clearance. While arriving at the above equations, the flow curvature effects have been neglected.

If the leakage path length is less than the large transition length, it is called intermediate orifice. A more accurate description of the terms - short, intermediate and long - orifices and their implication in leakage flow analysis are provided following Eq. 50. The intermediate orifice modelling presented here is based on boundary-layer analysis of steady, incompressible, entrance-region flow with uniform flow at inlet (Mookherjee, 2000).

Since the spool-bushing radial clearance is small in comparison to the spool diameter, flow analysis be-

tween two flat parallel plates separated by a distance r_c is acceptable in the present context. With reference to Fig. 5, the x-axis has been chosen to lie on the bottom wall and the y-axis has been chosen perpendicular to the x-axis. For a critically lapped spool valve, studied here, the length of the leakage path x equals the actual spool displacement. The three domain boundaries $x = 0$ and $y = 0$ and $r_c/2$ imply the inlet, the bottom wall and the mid-plane between the walls respectively. Only half the gap between the walls has been analyzed because of symmetry. The symmetry is an acceptable assumption on account of neglected flow curvature effects and considering the velocity of the bottom plate with respect to the fluid velocity to be negligible in the present analysis. The symbol $\delta(x)$ indicates the boundary layer thickness on the wall at any x. The symbol U_o has been used to represent the axial component of the velocity at inlet.

Considering a parabolic variation of $U(x,y)$ velocity within the boundary layer at any x satisfying the boundary conditions and integrating the boundary layer equations, one obtains

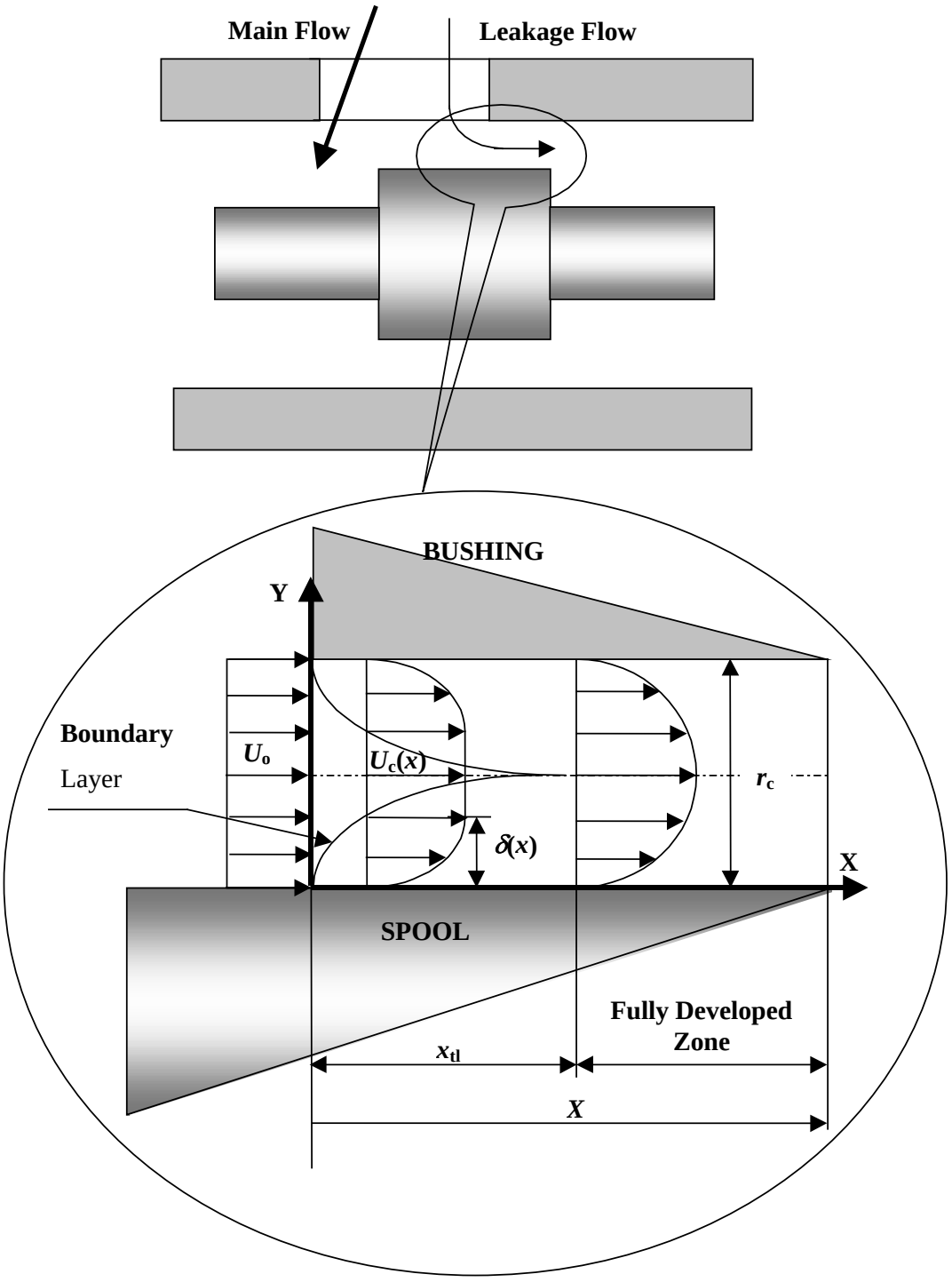

Fig. 4: *Boundary Layer Growth in Spool-Bushing Radial Clearance*

$$16\ln(1-\eta)+\frac{16\eta-7\eta^2}{1-\eta}=\frac{40x}{3r_c\,\mathrm{Re}_o} \tag{33}$$

where the boundary layer parameter

$$\eta = 2\delta/3\ r_c \tag{34}$$

and the Reynolds number

$$\mathrm{Re}_o = U_o\, r_c/\nu \tag{35}$$

with ν being the kinematic viscosity of the fluid.

Assuming $\eta < 1$ and $\frac{r_c\,\mathrm{Re}_o}{x} >> 1$, Eq. 33 yields

$$\frac{\delta}{x}=\sqrt{\frac{10}{3\mathrm{Re}_o}\frac{r_c}{x}} \tag{36}$$

It may be mentioned here that in the present analysis, the large transition length represents the distance from the entrance at which the boundary layers on the two walls meet at the mid-plane, as shown in the exploded diagram of Fig. 4. In formal duct flow analysis, this length is popularly called the entrance length. At large transition length, the boundary layers on the bounding parallel plates touch each other and the velocity profile attains the fully developed parabolic profile. Putting $\delta = r_c/2$ in the above equation, thus the large transition length can be obtained as

$$x_{tl}/r_c = 0.075\ Re_o \tag{37}$$

The value 0.075 in the above equation is in reasonable agreement with the value 0.071 obtained by Cebeci and Bradshaw (1977) following detailed numerical analysis of Navier-Stokes equation.

To find out the pressure-discharge relationship, the force equilibrium equation of the fluid control volume, within the radial clearance space as shown in the exploded diagram of Fig. 5, is considered. This relationship can be expressed as,

$$F_P = \left(\dot{h}_x - \dot{h}_o\right) + F_\mu \tag{38}$$

where, F_P is the net pressure force acting on the control volume, $\dot{h}_x$ is the rate of momentum efflux from the control volume at length x, $\dot{h}_o$ is the rate of momentum influx into the control volume and F_μ is the net viscous resistance offered to the flow.

Hence,

$$F_\mu = \int \mu_f \left.\frac{\partial u}{\partial y}\right|_{y=0} \frac{d_s}{2}\theta_P dx \tag{39}$$

Considering parabolic velocity profile and expression for the port width w given by Eq. 5, Eq. 56 can be simplified as:

$$F_\mu = \frac{24\rho Q^2\delta}{5r_c^2 w} \tag{40}$$

The rate of momentum transfer can be expressed as:

$$\begin{aligned}\dot{h}_x - \dot{h}_o &= \rho w\int_0^{r_c/2} u^2 dy - \frac{2\rho\, Q^2}{r_c w}\\ &= \frac{4\rho\, Q^2}{r_c w}\left[\frac{9r_c\delta - 10\delta^2}{\left(3r_c - 2\delta\right)^2}\right]\end{aligned} \tag{41}$$

with $$w = \frac{d_s}{2}\theta_P \tag{42}$$

Combining Eq. 38, 40 and 41, it is obtained that

$$F_P = \frac{2\rho\, Q^2}{r_c w}\left[f(\eta) + 3.6\right] \tag{43}$$

where

$$f(\eta) = \frac{3-5\eta}{(1-\eta)^2} \tag{44a}$$

and

$$\eta = \frac{2\delta}{3r_c} \tag{44b}$$

Now, $f(\eta)$ has a maxima of 3.125 at η = 0.2 and has a minima of 3 at η = 0 and 1/3. Hence $f(\eta)$ can be replaced by

$$f(\eta) = \overline{f} = 3\int_0^{1/3} f(\eta) d\eta = 3.08 \tag{44c}$$

Similarly, the pressure force can be expressed as,

$$F_P = \Delta P \frac{r_c}{2} w \tag{45}$$

Combining the above Eq. 43, 44c and 45 one can write:

$$\Delta P = \frac{23(\rho\mu x)^{1/2} Q^{3/2}}{r_c^{5/2} w^{3/2}} \tag{46}$$

A small transition length, x_{ts}, has been calculated in the steady-state performance analysis study such that at this length both the short and intermediate orifice formulations result in same pressure drop. Thus,

$$\frac{x_{ts}}{r_c} = \frac{\rho\ Q}{2116\ \mu\ w}\left[\frac{1}{C_{dp}^2\cos^2\alpha} - 1.5\right]^2 \tag{47}$$

The complete pressure discharge relationship for the leakage path is based on the above models along with consideration for entry and exit losses. The corresponding pressure-discharge relations, respectively for the short, intermediate and long orifice modes, are obtained as

$$\Delta P = \frac{1.5\rho}{w^2 r_c^2} Q^2, \text{ if } X \le -x_{ts} \tag{48}$$

$$\Delta P = \frac{1.5\rho}{w^2 r_c^2} Q^2 + \frac{23\left\{\rho\mu_f(-X)\right\}^{1/2}}{w^{3/2} r_c^{5/2}} Q^{3/2},$$
$$\text{if } -x_{tl} \ge X > -x_{ts} \tag{49}$$

and

$$\Delta P = \frac{1.5\rho}{w^2 r_c^2} Q^2 + \frac{23(\rho \mu_f x_{tl})^{1/2}}{w^{3/2} r_c^{5/2}} Q^{3/2} + \frac{12\mu_f (X + x_{tl})}{w r_c^3} Q \quad \text{if } X > -x_{tl} \tag{50}$$

The first term of the right hand side of the last two equations accounts for both the entry and exit losses, as stated earlier. These are the only loss component that has been considered in the present analysis corresponding to the short orifice mode given by Eq. 48. The second term in Eq. 49 and 50 accounts for the pressure drop in the entrance length. This adds up to represent the full drop in Eq. 49, corresponding to orifice length in the intermediate mode. In this case, the flow leaving the radial clearance space is short of acquiring the fully developed velocity profile, since the two wall boundary layers remain separated by a gap of uniform core flow about the mid-plane. The last term in Eq. 50 represents the pressure loss in the fully developed length.

Equations 49 or 50 are used to find out the discharge Q for a pressure drop ΔP depending upon the length of the leakage path. The average velocity corresponding to both the above cases are obtained as:

$$V = \frac{3}{5} \frac{15 r_c - 14\delta}{(3r_c - 2\delta)^2} \frac{Q}{w r_c} \tag{51}$$

The total flow force contribution due to the leakage flow can be expressed as:

$$F_S = -\rho (Q_2 V_2 \cos\alpha_2 + Q_3 V_3 \cos\alpha_3) \tag{52}$$

The subscripts used in the above equation indicate the port locations. When these subscripts are used in conjunction with Eq. 48 to 51, the effective leakage length is obtained as $X_2 = X_3 = x - u$, where u is the port underlap. The negative sign in Eq. 52 implies a force in the direction of spool displacement. Also, Eq. 4a has been used up to displacements for which the jet angle becomes equal to zero. For all displacement values beyond this, the jet angle is taken to be zero.

8 Simulation Algorithm

The simulation of the static performance is attempted using the SIMULINK software. A ramp input of the spool position, ranging from minimum to maximum spool displacement, is given to the spool valve flow solver. The effective spool displacement for the individual ports is then obtained from Eq. 1a and 1b. This SIMULINK solver solves for flow in the four ports of the spool valve corresponding to the given spool displacement x. The valve flow, control flow and leakage flow are obtained from the individual port flows as,

$$Q_v = Q_1 + Q_2 \tag{53a}$$

$$Q_c = Q_1 - Q_3 = Q_4 - Q_2 \tag{53b}$$

$$Q_L = Q_v - Q_c \tag{53c}$$

The flow solver also obtains the flow force contribution of the individual ports and sums them up to get the net F_S.

The current (c) evaluation loop involves finding zero of the static equilibrium function,

$$f(c) = F_S(x) + F_{mech}(x) - F_{em}(x, c) = 0 \tag{54}$$

The F_{em} and F_{mech} are evaluated in the LFM solver.

The flow solver algorithm is illustrated in Fig. 5. For a given spool dispalcement x, the effective spool port opening X_i in the four ports are calculated. The flow jet angle, α_i for each of the ports are then calculated. This angle is dependent on the X_i / r_c ratio (Merritt, 1967).

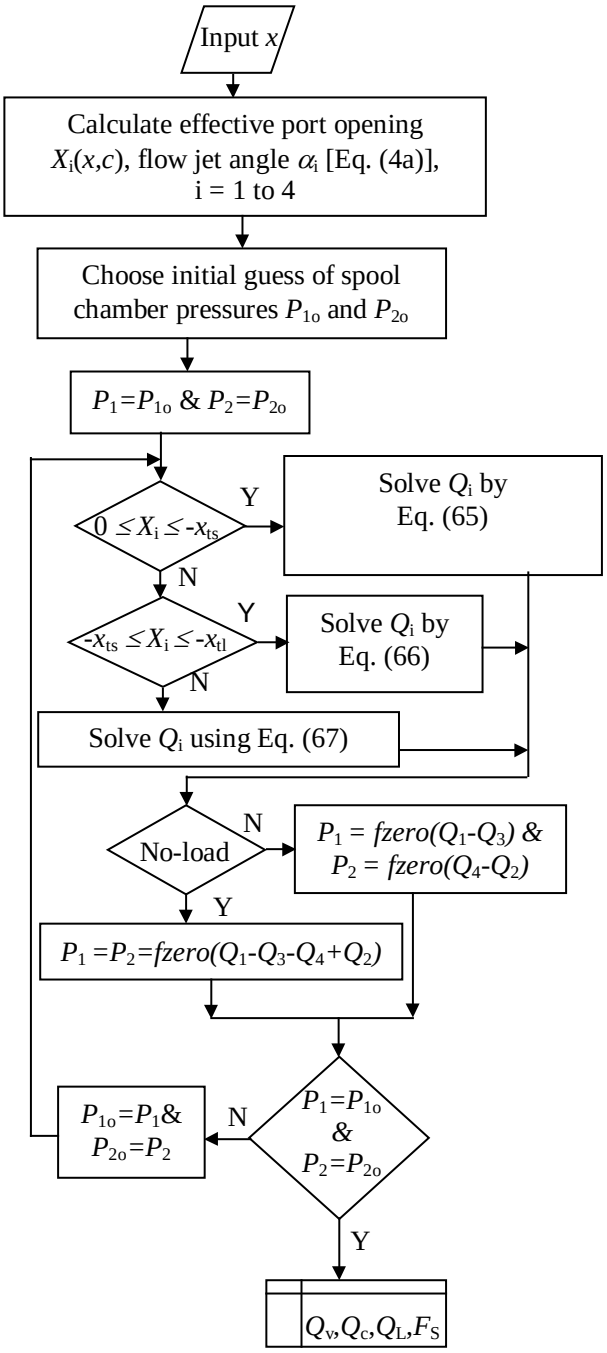

Fig. 5: *Spool Valve Flow Solver Algorithm*

8.1 Spool Valve Flow Solver Algorithm

The solution of the flow circuit starts with initial guesses for the spool chamber pressures P_1 and P_2, in order to calculate the discharge by appropriate one from Eq. 48 to 50 depending upon spool displacement. In case the discharge is calculated by solving the non-linear Eq. 49 or 50, the '*fzero*' function of MATLAB is invoked, starting with an initial guess of discharge.

If the DDV operates in no-load mode then the prevalent conditions, neglecting any pressure drop in the control ports, hold. These are:

$$Q_1\text{-}Q_3 = Q_4\text{-}Q_2 \tag{54a}$$

and

$$P_1 = P_2 \tag{54b}$$

Equation 54a is used to find out a value of $P_1 = P_2$.

If the DDV operates in locked actuator mode, then neglecting leakage past actuator piston, the following flow continuity equations are used to solve for P_1 and P_2 respectively:

$$Q_1\text{-}Q_3 = 0 \tag{55a}$$

$$Q_4\text{-}Q_2 = 0 \tag{55b}$$

Once the chamber pressures are obtained, the individual flows are used to evaluate Q_v, Q_c, Q_L and F_S.

9 Static Performance Results

Static performance configuration of the DDV implies a constant current in the coils, a constant position of the armature-spool assembly leading to a constant control flow. In the present analysis, a zero control flow implies the locked actuator mode and a zero load pressure drop implies the no-load mode.

Static performance results corresponding to the cases I, II and III presented in Section 7 are given below. These cases are also indicated in the figures of the following section by legends 1, 2 and 3 respectively.

9.1 DDV Characteristics with No-load Actuator

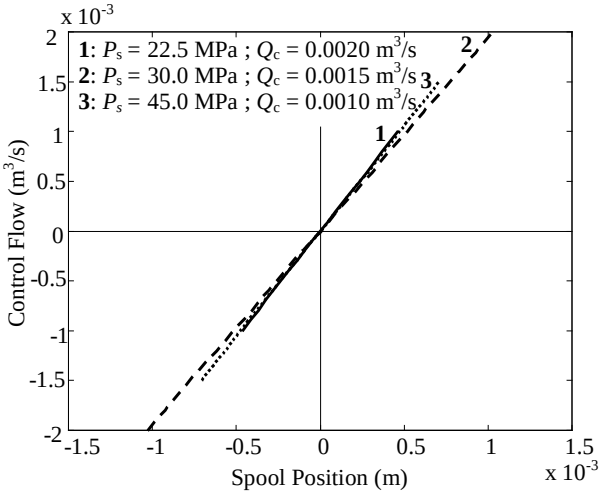

Fig. 6: *Spool Valve Flow Gain Characteristics*

Figure 6 depicts the spool valve flow gain defined as the variation of no-load control flow with spool position. For all the three designs, it can be seen that the valves deliver the respective rated control flows at corresponding designed strokes.

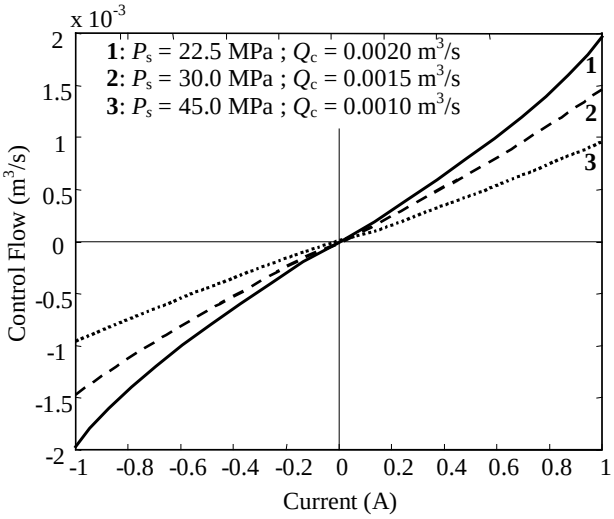

Fig. 7: *DDV Flow Gain Characteristics*

Figure 7 represents the valve flow gain, defined as the variation of the control flow with current. For all the three designs, it can be seen that the valves deliver the respective rated control flows at the rated current of 1A. This observation validates the design-level assumptions regarding negligible leakage flow at the rated no-load flow condition.

A comparison of Fig. 6 and Fig. 7 shows that the non-linearity present in the DDV flow gain curve is absent in the spool valve flow gain curve. So, one can conclude that the source of non-linearity in the DDV characteristic is due to the motor non-linearity and not due to jet-angle non-linearity.

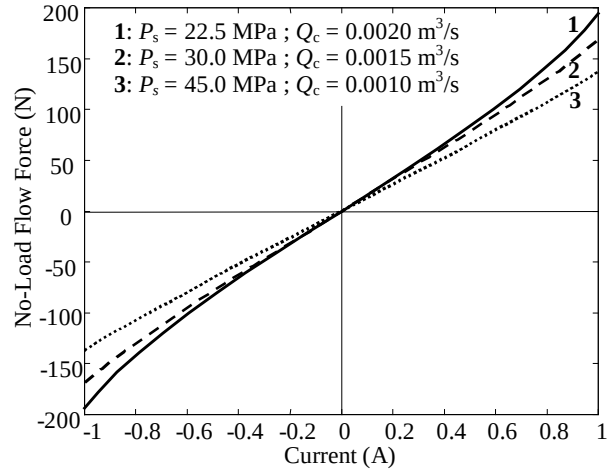

Fig. 8: *No-Load Flow Force Characteristics of a DDV*

Figure 8 represents the variation of steady-state flow force with current for a no-load actuator. It is observed that with an increase in supply pressure, the flow gain increases. This is understandable, since a smaller spool stroke permits the rated valve flow to

pass through for a larger supply pressure. The corresponding change in momentum is also higher due to an increase in flow velocity at the ports. This explains a higher steady state flow force for higher supply pressure in Fig. 8.

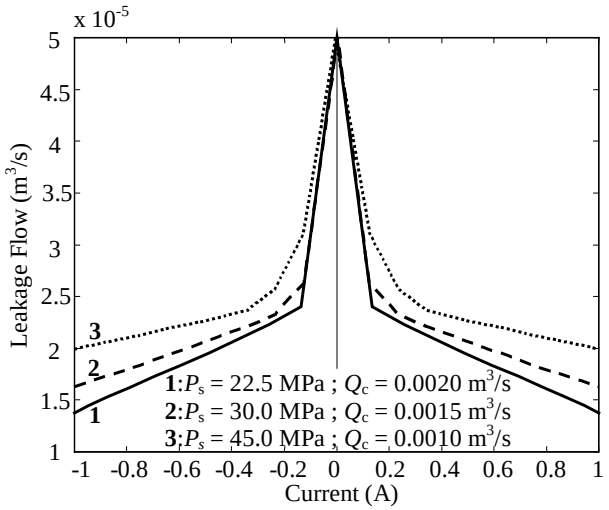

Fig. 9: *Leakage Flow Characteristics of a DDV*

In Fig. 9 the variation of leakage flow with spool displacement is shown. The leakage flow is observed to be largest at null and is consistent with the assumed design value for the maximum permissible leakage in the design. The leakage flow depends strongly on the length of the leakage flow path, which increases with spool displacement. As long as the length of the leakage flow path is lesser than the entrance length, non-linearity effect dominates over otherwise linear variation with leakage path length inherent in the laminar, fully-developed discharge modelling. The point of initiation of linear variation of leakage flow with spool displacement in Fig. 9 indicates the fully developed length of the respective cases.

9.2 DDV Characteristics with Locked Actuator

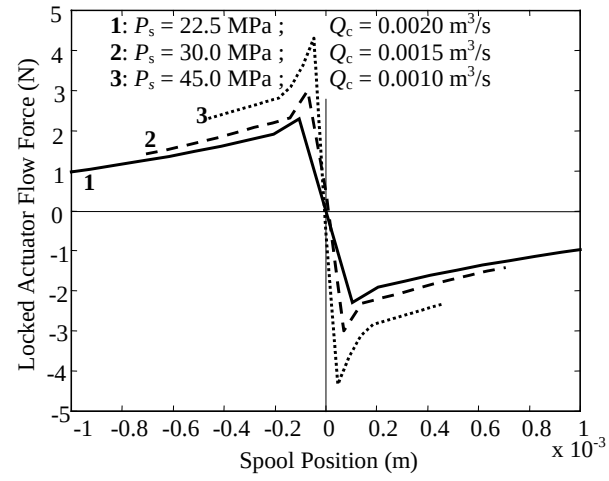

Fig. 10: *Locked Actuator Flow Force Characteristics* of a DDV

The locked actuator features a zero control flow, if the flow past the actuator piston is negligible. Figure 10 describes the variation of steady-state flow force with spool displacement for a locked actuator. A comparison between the cases of no-load and locked actuators reveals that the nature of variation of the steady state flow force is quite different. As mentioned in the previous section of a no-load actuator, essentially the main flow path dictates the steady state flow force. But, in case of a locked actuator, the discharge through all the metered ports are due to leakage and equal. Consequently flow at each port has significant contribution to the flow force. The contribution of the jets at the open metered ports is a centering flow force, whereas the contribution of the jets at the covered metered-ports is a de-centering flow force. In fact, a situation of increasing de-centering flow force is observed in the region of substantial jet-angle non-linearity. This happens by virtue of more axially oriented jets of higher velocity at the closing metered ports in comparison to opening metered ports. Beyond this region, the angular bearing of all the jets undergoes minor change with change in spool displacement. However, a decrease in flow results in a larger decrease in the de-centering flow force. This gives rise to the region of positive flow force stiffness, albeit a de-centering flow force.

Figure 11 represents the pressure gain characterisation of the valve, i.e., the variation of load pressure with spool stroke. A higher pump pressure rating is seen to generate a higher pressure gain.

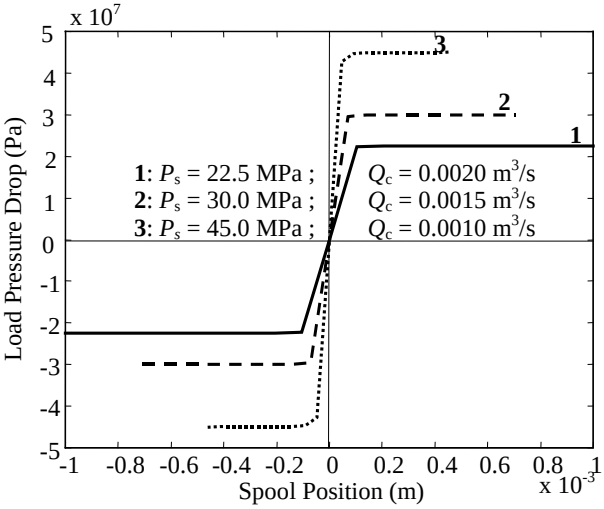

Fig. 11: *DDV Pressure Gain Characteristics*

9.3 Validation of Design Assumptions

In Fig. 12, the steady-state force characteristics of the DDV are presented corresponding to case I in Table 2, and spool displacement well beyond the mechanical limiter. The first intersection of the flow force curve and the spool driving force curve is indicated as the rated stroke in the figure. This prediction is in good agreement with the design stroke of $1.03 \cdot 10^{-3}$ m indicated in Table 2. As mentioned in Section 5.1 earlier, the intersection is in the drooping region of the spool driving force, which is the residue of the electromagnetic force generated by the LFM after overcoming the mechanical spring. The second intersection between the spool driving force curve and the flow force curve,

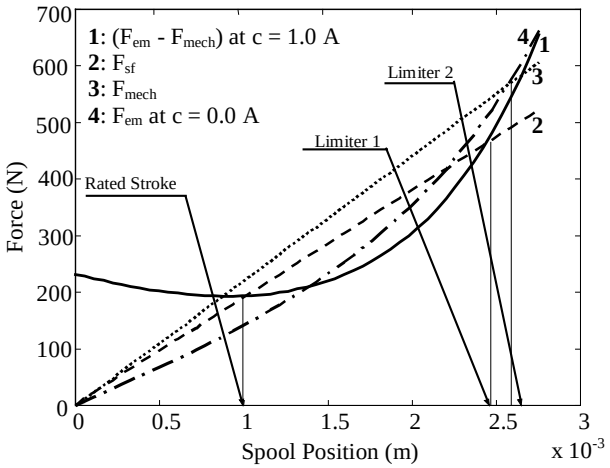

Fig. 12: *Force-Stroke Characteristics of DDV*

shown as Limiter 1 in Fig. 12, also agrees fairly well with the designed prediction of 2.5 $\cdot 10^{-3}$ m. A lower prediction of Limiter 1 by the static performance analysis can be attributed to the modification of flow and flow forces in this analysis due to leakage flow, which was neglected in formulating the design algorithm. A large separation between the two intersections is also consistent with the design philosophy explained in Section 5.1 following Eq. 46. The position of Limiter 2 in Fig. 12 corresponds to the consideration of armature retraction by the mechanical spring alone. This prediction also shows a satisfactory agreement with the design prediction of 2.57 $\cdot 10^{-3}$m. The comparison between the predictions of the design and static performance analysis presented here as well as earlier in Fig. 6, 7 and 9, indicate satisfactory validation of the assumptions used in the design procedure.

10 Sensitivity Analysis Results

The valve for which the sensitivity analysis has been carried out here corresponds to a design with pump pressure of 22.5 MPa. The basic specifications and sizes of the DDV are presented as case I in Tables 1 and 2.

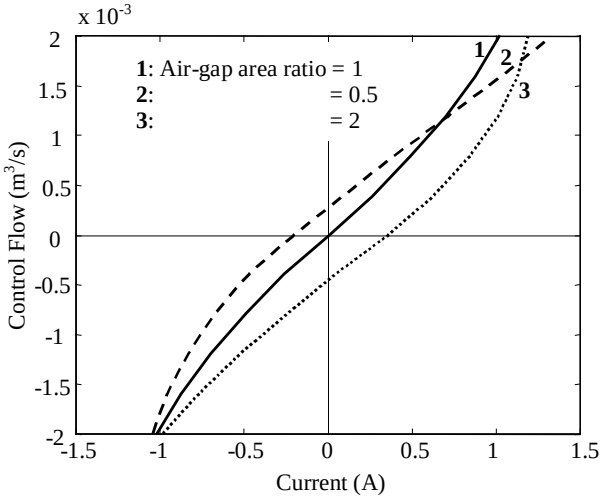

Fig. 13: *Sensitivity of Air-gap area ratio on DDV Flow Gain*

Figure 13 represents the effect of ratio of the two tractive air-gap areas on flow gain for three different values of 0.5, 1 and 2. The unequal tractive air-gap areas are analyzed with one having double the designed size and the other having half the designed size. For each of such cases, when the armature is at its geometric null (x = 0), the fluxes through the two air-gaps are unequal due to unequal path reluctances. This results in a non-zero current in the coil, resulting in a corresponding null bias. Change in flow gain due to unequal tractive air-gap areas is because of reduction in force capability of the motor corresponding to increase in reluctance in one tractive gap. The equality of gain and reversal of the null bias corresponding to the unequal area ratios considered is due to their reciprocal variations. The figure indicates that the designed valve delivers the rated flow at the rated current.

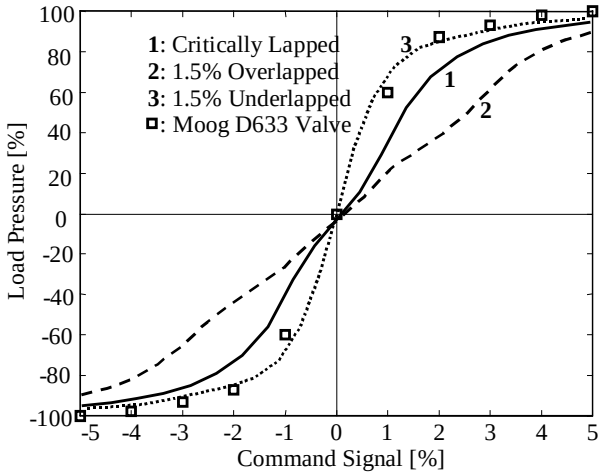

Fig. 14: *Sensitivity Analysis of Lap Condition on DDV Pressure Gain*

Figure 14 presents the sensitivity analysis of valve lap condition on pressure gain variation of the DDV. A major objective of this figure is to present a validation of the present design and static performance algorithm against the Moog Series D633 DDV.

Design results corresponding to these specifications as obtained from the present algorithm have already been presented in Table 2 as case IV. The magnetic material specifications corresponding to the LFM has been taken as identical with the earlier cases. This was done as no corresponding material specification could be obtained from the manual of the Moog valve.

In Fig. 14, the load pressure, that is developed across the actuator piston under locked condition, has been presented as a percentage of the pump supply pressure. The command signal is in terms of percentage of the rated current. Besides the pressure gain corresponding to the designed critically lapped valve, results for 1.5% underlapped and overlapped valves are also presented in the figure. All these results have been presented as continuous curves. However for the sake of clarity, the performance results of the Moog valve, as available in the literature, have been presented as discrete points in the same figure.

The sharp null response of the underlapped valve is due to sharp near-null variation of the jet angle. A gradual decrease in sharpness of the valve response has

been observed in the order of underlapped to critically lapped to overlapped configurations. This is due to a gradual shift of the region of sharp variation of the jet angle away from the valve null. The present predictions corresponding to the underlapped and critically lapped valve configurations are in fairly good match with the Moog valve. The configuration of these valves are very much similar with some deviation in the motor. The magnet specifications were not given. A Samarium-Cobalt magnet was used in the present work, and a design abiding to Moog specifications was carried out. It should be borne in mind that the inner details of the Moog valve which were not available from literature were evaluated as design outputs. Also the objective of the present study was not to reproduce the Moog sizes, but to compare the performances of the present design and the Moog valve. A performance comparison in non-dimensional was carried out, which is a standard practice for validating a developing hardware with incomplete knowledge of inner detail. The performance prediction of the designed valve is found to be in excellent agreement with that of the Moog valve. In absence of any other results in the literature pertaining to a DDV, a more direct validation of the present methodology could not be undertaken at this stage.

11 Conclusions

A systematic design algorithm on the basis of no-load and locked actuator static performance model of a DDV has been developed in the present study. Exploitation of the force-stroke diagram for constant current in formulating important design constraints is the major contribution of the present exposition. The design involves some simplifying assumptions, over and above the performance model. These design-level assumptions were found to be acceptable through matching with static performance results.

The present investigation involves a sensitivity study of some geometric sizes on the no-load and locked actuator static performances. It has been found that radial clearance and lap condition of the valve has critical bearing on small-signal performance of the valve. A mismatch in the two tractive air gaps at valve null is a source of null bias of the valve. Port shaping was found to be a possibility to counteract the motor non-linearity. A good agreement of non-dimensional valve performance between the present design and a Moog series D633 DDV clearly established the different considerations that led to the design algorithm. As a continuation of the present effort, a design updation considering the static performance of a slewing actuator under different load conditions should be considered. This updation study forms the prerequisite of experimental performance measurement of the valve designed following the complete static performance considerations.

The major theoretical contribution of the present analysis lies in obtaining the pressure-discharge relationship in the leakage path. This analysis can also be applied in case of laminar flow through transmission lines of short length.

Nomenclature

A_f	area of fixed air-gap	[m²]
A_{mi}	cross-sectional area of i^{th} magnet (i = 1,2)	[m^2]
A_{pi}	flow area of i^{th} port opening (i = 1 to 4)	[m^2/s]
A_{ti}	area of i^{th} tractive air-gap (i = 1,2)	[m²]
B_o	residual flux density of permanent magnets	[Wb/m²]
c	current	[A]
C_{dp}	port discharge coefficient	[-]
c_{max}	maximum current	[A]
c_p	clearance around push rod	[m]
c_r	rated current	[A]
C_{vp}	port velocity coefficient	[-]
d_{clbi}	inner diameter of coil bobbin	[m]
d_{clbo}	outer diameter of b	[m]
d_{clw}	diameter of coil wire	[m]
i	inter-land diameter	[m]
d_p	push rod diameter	[m]
d_s	spool land diameter	[m]
F_{cs}	chip shear force	[N]
F_{em}	electromagnetic force	[N]
F_{mech}	mechanical spring force	[N]
F_S	total steady-state flow force	[N]
F_{Si}	steady-state flow force contribution of the i^{th} port	[N]
g_f	fixed air-gap thickness	[m]
g_o	tractive air-gap thickness at null	[m]
H_o	coercivity of permanent magnets	[AT/m]
K_{mech}	mechanical spring stiffness	[N/m]
L_a	length of armature	[m]
L_{cl}	length of coil bobbin	[m]
L_{mi}	length of i^{th} magnet (i = 1,2)	[m]
M_c	magnetomotive force of coils	[AT]
M_i	magnetomotive force of i^{th} magnet (i = 1,2)	[AT]
M_o	magnetomotive force of magnets at null	[AT]
N	total number of turns in coil bobbins	[-]
n_{cb}	number of coil bobbins	[-]
n_P	number of port cuts	[-]
P_i	pressure in the i^{th} spool chamber (i = 1,2)	[N/m^2]
P_L	actuator load pressure drop	[N/m^2]
P_R	return pressure	[N/m^2]
P_S	supply pressure	[N/m^2]
Q_{ci}	control flow in the i^{th} actuator chamber	[m^3/s]
Q_i	flow through i^{th} port opening (i = 1 to 4)	[m^3/s]
Q_L	total leakage flow	[m^3/s]
Q_v	total valve flow	[m^3/s]
r_c	spool-bushing radial clearance	[m]
Re_o	leakage flow Reynolds number	[-]
R_f	reluctance of fixed air-gap	[AT/ Wb]
R_{max}	maximum resistance of the coil	[Ω]
R_{mi}	reluctance of i^{th} magnet (i = 1,2)	[AT/ Wb]
R_o	reluctance of tractive air-gaps at null	[AT/ Wb]
R_{ti}	reluctance of i^{th} tractive air-gap	[AT/

	(i = 1,2)	Wb]
t_a	thickness of armature	[m]
u	port lap with spool at null	[m]
V_i	velocity of flow through i^{th} port opening (i = 1 to 4)	[m/s]
x	spool displacement	[m]
X_i	effective opening of the i^{th} port (i = 1,2)	[m]
x_s	steady-state displacement of spool-armature from null	[m]
x_{tl}	long transition length	[m]
x_{ts}	short transition length	[m]
α_i	flow jet angle at the i^{th} port opening (i = 1 to 4)	[^{o}]
δ	boundary layer thickness	[m]
ΔP	pressure drop in leakage path	[Pa]
η	boundary layer parameter	[-]
μ	permeability of air	[H/m]
μ_f	fluid viscosity	[N·s/m²]
ν	kinematic viscosity of fluid	[m^2/s]
θ_p	total port wrap angle	[^{o}]
ρ	fluid density	[kg/m^3]
ρ_c	resistance per unit length of coil wire material	[Ω/m]
τ_{cs}	chip shear strength	[N/m²]
ψ_c	magnetic flux through coils	[Wb]
ψ_i	magnetic flux through i^{th} magnet (i = 1,2)	[Wb]
ψ_o	Magnetic flux through magnets at null	[Wb]
ψ_{ti}	Magnetic flux through i^{th} tractive air-gap ψ (i = 1,2)	[Wb]

References

Bird, R. B., Stewart, W. E., Lightfoot, E. N. 1960. *Transport Phenomena*. John Wiley & Sons, New York.

Cebeci, T. and **Bradshaw, P.** 1977. *Momentum Transfer in Boundary Layers*. McGraw-Hill, New York.

Jones, J. C. 1997. Developments in design of Electro-hydraulic Control Valves from their initial design concept to present day design and applications. *Workshop on Proportional and Servovalves.* Monash University, Melbourne, Australia.

Lee, S.-Y. and **Blackburn, J. F.** 1952. Contributions to Hydraulic Control – 1 Steady-State Axial forces on Control-Valve Pistons. *Trans. ASME*, pp. 1005-1011.

Merritt, H. E. 1967. *Hydraulic Control Systems*. John Wiley & Sons, New York.

Miller, F. G. 1993. Direct drive control valves and their applications. *C474/014,IMechE*, pp. 1-17.

Moog, W. C. 1965**,** U.S. Patent 2,625,136.

Mookherjee, S. 2000. Design and Sensitivity Analysis of a Single-Stage Electro-Hydraulic Servovalve. *Proceedings of 1st FPNI-PhD Symposium Hamburg 2000*, Hamburg, pp. 71-88.

Saha, R., Mookherjee, S., Sanyal, D. and **Majumdar, K.** 1998. Performance Analysis of DDV for Different Forms of Input Signal. *3rd National Conference on Fluid Machinery*, India, pp. 189-194.

Steed, D. J. 1993. Direct drive actuation for primary flight control. *C474/020, IMechE*, pp. 17-22.

Yeaple, F. 1996. *Fluid Power Design Handbook*. Marcel Dekker Inc., New York.

Saikat Mookherjee
Born on September 1968 in Calcutta (India). Graduated in 1991 from Mechanical Engineering department, Jadavpur University, Calcutta. In 1993, completed his Masters thesis from Indian Institute of Science, Bangalore (India). Since 1994 joined as a faculty in Mechanical Engg., Jadavpur University. Member of the NEPTUNE Research Group in Mechanical Eng. Dept., Jadavpur University since 1994. Presently working on fluid power devices

Sanjib Acharyya
Born on August 1965 in Calcutta (Inida). Study of Mechanical Engineering at Shibpur B.E. College (Calcutta University) in 1987. Post-graduation from Shibpur B.E. College (Calcutta University) in 1989. Since 1991 joined as a faculty in Mechanical Engg., Jadavpur University. Member of the NEPTUNE Research Group in Mechanical Eng. Dept., Jadavpur University. Presently working on servo-valve design and fracture mechanics.

Kamalesh Majumdar
Born on August 1944 in Calcutta (Inida). Graduated in 1966 and received Master's degree in 1969 from Mechanical Engineering department, Jadavpur University, Calcutta. Since 1967 joined as a faculty in Mechanical Engg., Jadavpur University. Founder member of the NEPTUNE Research Group in Mechanical Eng. Dept., Jadavpur University. Presently working on fluid power and control.

Dipankar Sanyal
Born on May 26, 1962 at Calcutta (India) Obtained Mechanical Engineering degrees: Bachelors from Jadavpur University at Calcutta and Masters degree from Institute of Science at Bangalore. Completed doctoral thesis on spray combustion analysis at the Indian Institute of Science at Kanpur. Faculty in Mechanical Engineering Department, Jadavpur University since 1991. An active researcher in the NEPTUNE group in the areas of CFD, Spray Combustion and Fluid Power Control analyses.